

Characterization of a novel plastic scintillation detector for in vivo electron dosimetry

Cornelius J. Bauer^{1,*}, Frank Schneider¹, Ida D. Göbel¹, Hans Oppitz¹, Frank A. Giordano^{1,2,3}, Jens Fleckenstein¹

¹ *Department of Radiation Oncology, University Medical Centre Mannheim, Heidelberg University, Germany*

² *DKFZ-Hector Cancer Institute, University Medical Centre Mannheim, Mannheim, Germany*

³ *Mannheim Institute for Intelligent Systems in Medicine (MIISM), Medical Faculty Mannheim, Heidelberg University, Mannheim, Germany*

**corresponding author*

Cornelius J. Bauer¹, *Ph.D.*

Department of Radiation Oncology

University Medical Centre Mannheim, Heidelberg University

Email: Cornelius.Bauer@umm.de

KEY WORDS

Dosimetry, plastic scintillation detector, electron beam, surface dose

Abstract:

Introduction: Real-time dosimetry of surface dose in electron beams has not been widely established yet, but offers further insights for radiotherapy. Plastic scintillation detectors (PSD) promise high spatial resolution and real-time dosimetry with minimum perturbation of the radiation field. This study characterizes a novel PSD for the first time in an electron beam with the purpose of in-vivo dosimetry.

Methods: Dosimetric characterization and dual channel Cherenkov correction were investigated using reference ionization chambers. Percentage depth dose curves, lateral profiles and output-factors were compared to reference ionization chambers. Surface doses were measured on solid water and on an anthropomorphic phantom and compared to ionization chamber and radiochromic film measurements.

Results: The investigated PSD demonstrated clinically acceptable linearity, dose rate independence, isotropy and reproducibility (total variation <2%). The detector measured R_{50} and R_{80} to 0.5 mm accuracy and lateral profiles with a mean absolute error below 1.5%. Small field measurements were within 2% of reference ionization chamber. Surface dose measurements had a relative deviation of 0.9% from ionization chamber and 2.6% from radiochromic film measurements.

Conclusion: The PSD investigated in the present study is suitable for clinically acceptable electron beam dosimetry and provides accurate surface dose measurements in phantom experiments. It has the potential to be used in vivo for real-time dosimetry.

1 Introduction:

Radiotherapy is one of the most common modalities for advanced cancer treatment^{1, 2}. Accurate knowledge of the energy dose delivered to the patient is essential to ensure adequate therapeutic results while sparing healthy tissue. Dosimetry also plays a critical role in machine and patient-specific quality assurance as well as in vivo validation during irradiation. For electron beam radiotherapy, this becomes particularly important, as manual patient setup and beam collimation can markedly affect the total dose as well as the shape of the depth-dose curve^{3, 4}. Hence, in vivo dosimetry can provide valuable information to verify a correct treatment delivery.

Approaches for in vivo dosimetry on the patient surface include the use of radiochromic films^{5, 6, 7}, MOSFET^{8, 9} and diodes^{10, 11}. While all these approaches have their strengths and weaknesses, a real-time non-perturbative measurement that is independent of dose rate, energy and direction is not feasible with any of these approaches^{9, 10}. For absolute dosimetry, ionization chambers provide accurate results but cannot be used for in vivo applications, as they significantly perturb the beam during measurement and cannot be used on patient surfaces¹². Hence, different detectors need to be investigated for electron in vivo dosimetry.

Plastic scintillation detectors (PSDs) have been introduced as active detectors that can be constructed in a compact design¹³⁻¹⁵. Commercially available PSDs are often used for high spatial resolution in stereotactic body radiotherapy (SBRT) applications¹⁶ or in ultra-high dose rate (UHDR) conditions such as FLASH radiotherapy¹⁷⁻²⁰ due to their high temporal resolution. PSDs are claimed to be water-equivalent and thus promise minimal disturbance of the beam during measurement. In addition, they provide real-time dose readout, which is crucial for online-monitoring in vivo dosimetry. The downside of PSDs is the need to correct for Cherenkov light leading to measurement uncertainties and limited signal-to-noise ratio^{21, 22}.

The Blue Physics Model 11 plastic scintillation detector (SD, Blue Physics, Tampa, USA) is a novel PSD that offers high spatial and temporal resolution²³. Characterization in a photon beam showed promising dosimetric results²⁴. However, no characterization in electron beams has been published, yet. Furthermore, the use of minimally perturbative PSDs for surface dose measurements has not been investigated so far.

In the present study, we characterized SD for the first time in an electron beam and evaluated its potential for accurate electron beam dosimetry. We verified that measurements with SD had minimal impact on the electron beam facilitating the use in vivo. Finally, we investigated the accuracy of surface dose measurements with SD and doses underneath a clinically realistic bolus material.

2 Materials and Methods

2.1 Detector and Experimental Set-up

SD consists of a plastic scintillator, an optical fiber and an acquisition unit. The included software BlueSoft was used for all data acquisition first processing steps. Fig. 1 illustrates the detector composition. SD uses a dual-channel approach to correct for Cherenkov light that inevitably occurs through the partial irradiation of the optical fibers. A second, nearly identical fiber only detects this Cherenkov light and is subtracted from the sensor signal using the so called adjacent channel ratio (ACR). This quantity corresponds to the Cherenkov light ratio used from other PSDs²⁵.

Manufacturer specifications indicate a sensitive volume of 0.785 mm³ (cylinder of 1 mm length and diameter) and a minimum integration time of 300 μ s. All measurements in this study were performed using an integration time of 750 μ s. For evaluation, averaging was used to achieve an effective temporal resolution of 3 ms.

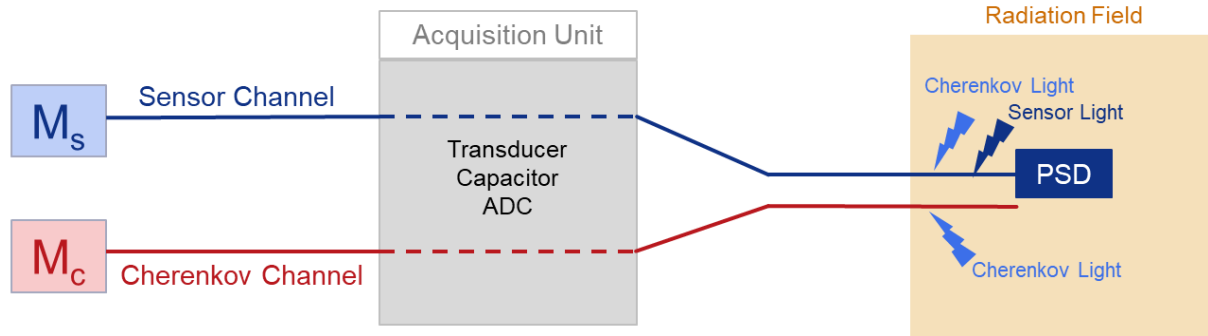


Fig. 1: Schematic detector set-up of SD. Light generated in the plastic scintillator as well as Cherenkov light is acquired. Using a secondary channel that only measures Cherenkov light, isolation of the sensor light is feasible.

All measurements were performed at a medical linear accelerator (Linac, Synergy, Elekta AB, Stockholm, Sweden) with available electron energies from 6 to 12 MeV. Dose rates were chosen in four levels between 50 and 400 MU/min. 6×6 cm² or 10×10 cm² electron applicators were used, depending on the required field size. Further beam collimation was performed via rectangular Roses Metal (MCP-96) inserts. Source-surface distance (SSD) was 100 cm and the measurement depth was chosen to be reference depth z_{ref} , at the surface or below 1 cm of bolus material depending on the experiment²⁶.

Water phantom measurements were performed using a water phantom (MP3-XS, PTW, Freiburg, Germany). Relative dosimetric measurements were performed in a water-equivalent RW3 slab (PTW Freiburg, Germany).

Radiochromic films (RF, Gafchromic EBT-XD, Ashland Specialty Ingredients, NJ, USA) were evaluated 24 hours after irradiation using in-house standardized protocols to gain 16 bit red channel data R . Color-to-dose calibration in the red channel was performed using data from an Advanced Markus ionization chamber (AM, Type 34045, PTW, Freiburg, Germany) and a regression with the function:

$$D_{RF} = a + \frac{b}{\log R - c} \quad (1)$$

Model parameters were $a = -27.01$ Gy, $b = 55.44$ Gy, $c = 8.75$. The mean absolute relative error was 3.0%, $R^2 = 0.9994$ ²⁷.

2.2.1 ACR Measurement

To determine the detector-specific ACR value, the vendor-recommended method was used. For field sizes from 2×2 cm² to 20×20 cm², the dose equivalent to 200 MU in a 10×10 cm² field was determined using AM. The theoretical signal in the sensor channel M_s can be expressed in terms of the Dose D , the calibration factor f_{cal} , the ACR and the signal in the Cherenkov channel M_c :

$$M_s = \frac{D}{f_{cal}} + ACR \times M_c. \quad (2)$$

Measuring M_s and M_c for each field size three times, the ACR was determined as the slope of a linear regression. The ACR-corrected signal was denoted as

$$M = M_s - ACR \times M_c \quad (3)$$

and used for all further analysis.

2.2.2 Dosimetric Characterization

The characterization of SD in an electron beam consisted of a series of measurements. First, the dose linearity was determined for all available energies by irradiating the detector with varying doses from 1 to 1000 MU. With a linear relation from energy dose D as measure by AM and detector reading M , calibration was performed combining equation (2) and (3):

$$D = f_{cal} \times M \quad (4)$$

Dose rate dependence was measured from 50 to 400 MU/min and for all energies, analyzing for trends or variations. The short-term repeatability was determined using ten-fold delivery of a 10×10 cm², 10 MeV field within a few minutes.

Finally, the isotropy of SD was determined using all energies and irradiation from all cardinal directions. For this, the detector was rotated in 90° increments using external markers.

2.3 Percentage Depth Dose Curves and Transversal Profiles

Percentage depth-dose-curves (PDDs) were acquired using SD and AM as reference. Ionization-to-dose conversion was performed according to TG-51 protocol²⁶. PDDs were measured for each energy from depth $z = 100$ mm to the water surface $z = 0$ mm.

Analysis of the PDDs is based on the depth of maximum dose R_{max} as well as the depth of dose fall-off to 80/50% called R_{80} and R_{50} , respectively.

To evaluate the potential for in vivo-dosimetry, the perturbation of SD in the beam was investigated by acquiring a PDD with AM natively and with SD directly above the water surface. Ideally, less than 1 mm shift and no further distortion of the PDD would be expected.

The transversal profiles for each energy available were measured in depth $z = 0$ cm and 1 cm (as compared to surface measurement and underneath 1 cm bolus). A 6×6 cm² field was measured inline (IL) and crossline (CL) with a scan length of 12 cm. An ionization chamber (Semiflex3D Type 31021, PTW, Freiburg, Germany) served as reference for profile measurements. For evaluation, the mean absolute error (MAE) and mean error (ME) are considered across the scan length.

2.4 Small Field and Output-Factor Measurement

Treatments for superficial target often require small electron fields and hence further patient specific collimation. SD offers the possibility to measure small fields without further correction factors. For validation, the central dose at in 1 cm depth for field sizes from 7×7 cm² to 3×3 cm² was determined using SD and AM. Normalization to the dose of the 7×7 cm² field yielded the comparable output-factor (OF).

2.5 Surface Dose Measurement

Surface dose measurements were performed twofold: First, SD measurements were compared to AM at the surface of the RW3 slab phantom and underneath 1 cm of bolus material (Bolx-I, Action Products, Hagerstown, MD, USA). Second, the dose at surface and underneath 1 cm of bolus was measured with SD on an anthropomorphic thorax phantom (002LFC, Sun Nuclear, Norfolk, VA, USA). Due to the curved surface, RF was used as a dosimetric reference for this set-up. All surface dose measurements were performed using 200 MU in a 6×6 cm² radiation field for all available energies. The experimental set-up for surface dose measurements is shown in Fig. 2.

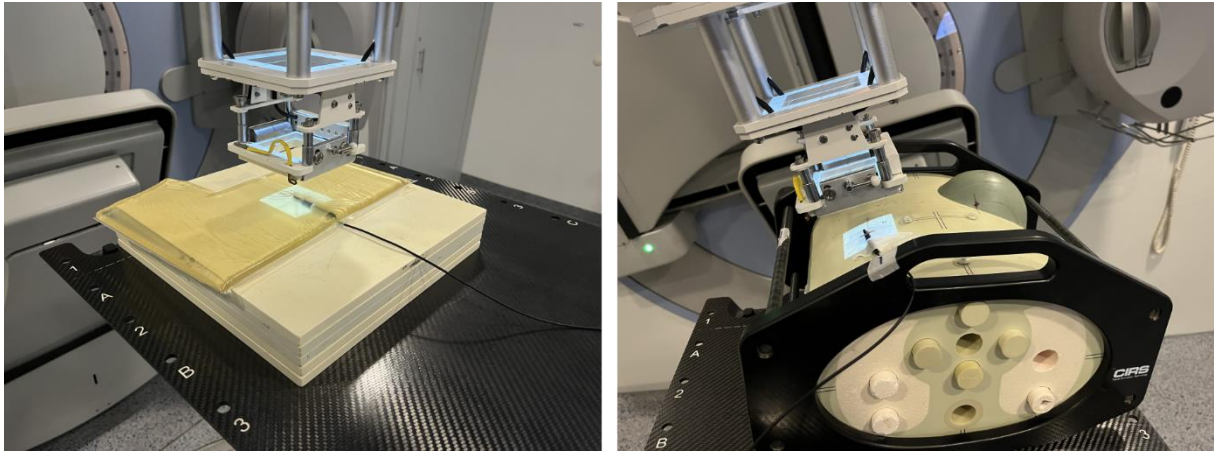


Fig. 2: Experimental set-up for surface dose measurements. Left: RW3 slab phantom with 1 cm bolus material. Gantry angle 0°. Right: Anthropomorphic phantom without bolus material, gantry angle 345°. SD is placed on the surface or right underneath bolus.

3. Results

3.1 ACR and dosimetric characterization

The measured ACR was (0.916 ± 0.013) , which is in line with the specifications by the manufacturer. This value was used for the isolation of the dose-proportional SD signal for all following measurements.

The dose linearity of SD was 1.3%. For dose deliveries below 5 cGy, the linearity was better than 1.0%. The variation in detector response over different dose rates was below 1.0%. There was no observable trend in the data regarding the energies or dose rate. The short-term repeatability was measured with 10 MeV electrons and was below 0.3%. There was no observable trend in the data during the acquisition time. The isotropy was 0.8%. Tab. 1 summarizes the numerical values obtained in the detector characterization. Concerning deviations, the standard deviation is shown. All relevant properties were within 1.5%. A squared summation of all individual standard deviations (assuming independence) yielded a total standard deviation of 1.8%.

Tab. 1: Detector characterization. For each detector property, the measurement procedure and obtained value or standard deviation are given.

Property	Measurement	Value/Standard deviation
ACR	ACR measurement using different field sizes	0.916 ± 0.013
Calibration f_{cal}	Calibration against a reference ionization chamber (AM)	$(2.29 \pm 0.01) \text{ cGy}/\mu\text{C}$
Linearity	Detector signal from 1 to 1000 MU	1.3%
Dose rate dependence	Detector reading for 100 MU at varying dose rates (50-400 MU/min)	1.0%
Repeatability	Detector reading for the same delivery settings (10 \times)	0.3%
Isotropy	Detector signal given rotation around the central axis	0.8%

3.3 Depth-Dose Curves and Water Equivalence

A comparison of PDD measured by SD and AM is shown in Fig. 3. For all available energies, the PDDs align well and only small deviation near the phantom surface are observed. Tab. 2 summarizes the differences between SD and AM (R_{max} , R_{80} and R_{50}). These values differ by less than 1.0 mm. Only R_{max} (determined in the plateau region) for 12 MeV is markedly shifted by 3.4 mm.

For the purpose of in vivo dosimetry, it is essential that SD within the radiation beam does not relevantly change the dose distribution within the patient. Comparing PDD measured with AM natively and with SD passively in the beam, a shift towards smaller ranges was observed. An analysis of R_{50} and R_{80} indicated shifts of 0.6 ± 0.4 mm in line with the thickness of SD.

Tab. 2. Comparison of PDD measurements based on range parameters for AM and SD.

Range	Incident electron beam energy			
	6 MeV	8 MeV	10 MeV	12 MeV
R_{max} [mm] (SD /AM)	14.0/13.5	17.4/16.5	22.5/22.0	28.4/25.0
R_{80} [mm] (SD /AM)	20.5/20.5	26.9/27.0	33.5/33.5	40.9/41.0
R_{50} [mm] (SD /AM)	25.0/24.5	32.4/32.5	39.5/40.0	48.4/48.0

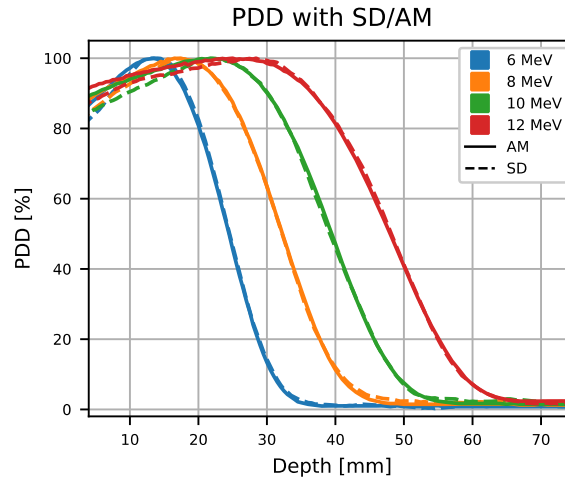


Fig. 3: PDD comparison measuring with AM (solid line) and SD (dashed line). The curves align for all energies.

3.4 Transversal Beam Profiles

Profile measurement were performed for each energy and scan direction (IL and CL) in the transversal plane. MAE and ME are shown in Tab. 3. indicating the difference between SD and ionization chamber. MAE was between 0.5% and 1.5% for all measurements. For IL direction MAE values were 0.5-0.8% higher than for CL. The ME (indicating any systematic shifts between the two measurements) ranged from -0.7% to 0.9%. There were no trends or shifts between SD and ionization chamber measurements.

Tab. 3: Mean absolute error (MAE) and mean error (ME) for profile measurements comparing SD and ionization chamber. Comparison at different energies for measurement depth 0 cm and 1 cm.

Direction	Incident electron beam energy			
	6 MeV	8 MeV	10 MeV	12 MeV
IL (0 cm)	1.4%/0.9%	1.5%/0.8%	0.9%/-0.4%	0.7%/-0.2%
CL (0 cm)	0.7%/-0.2%	0.7%/-0.5%	0.7%/-0.2%	0.9%/-0.7%
IL (1 cm)	1.1%/0.6%	1.0%/0.5%	0.9%/-0.3%	0.9%/-0.4%
CL (1 cm)	0.6%/0.0%	0.5%/-0.3%	0.6%/0.0%	0.6%/0.0%

Fig. 4 shows a representative profile (6 MeV in CL direction). Visually, the profiles aligned both on the surface as well as in 1 cm depth. The difference plots underlined the noise-like nature of the differences. In these profiles, no difference above 2% was observed.

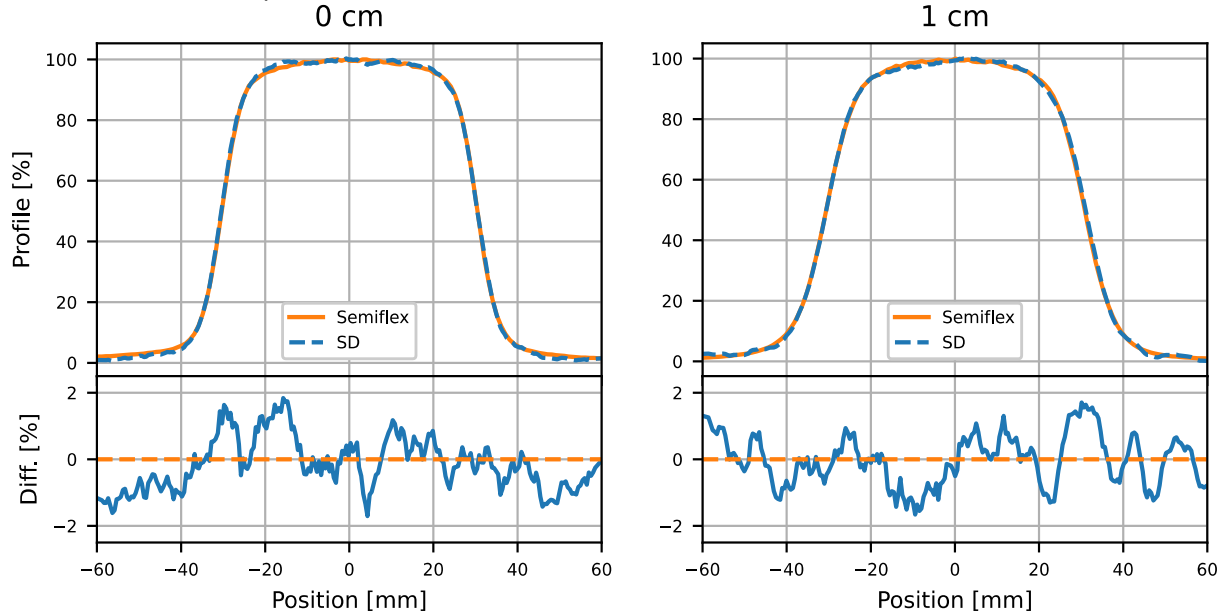


Fig. 4: Representative Profile of 6 MeV electrons in CL direction at the surface (0cm, left) and in 1cm depth (right). SD and ionization chamber data are shown together with the difference plot. Visually, the profiles aligned and the differences were noise-like without trends or shifts. No difference above 2% was observed.

3.5 Small Field and Output-Factor Measurement

For the use of SD inside small fields, SD should measure the output factor curve without further correction. Fig. 5 shows the OF curve for all energies measured with SD and AM. For field sizes from $3 \times 3 \text{ cm}^2$ to $7 \times 7 \text{ cm}^2$, SD and AM align very well with mean deviation of $(0.4 \pm 0.8)\%$ for all energies.

The field size dependance of the OF is most prominent for 6 MeV where total variation of 10% is observed. For 12 MeV only 4% difference in OF is measured between the largest and the smallest field.

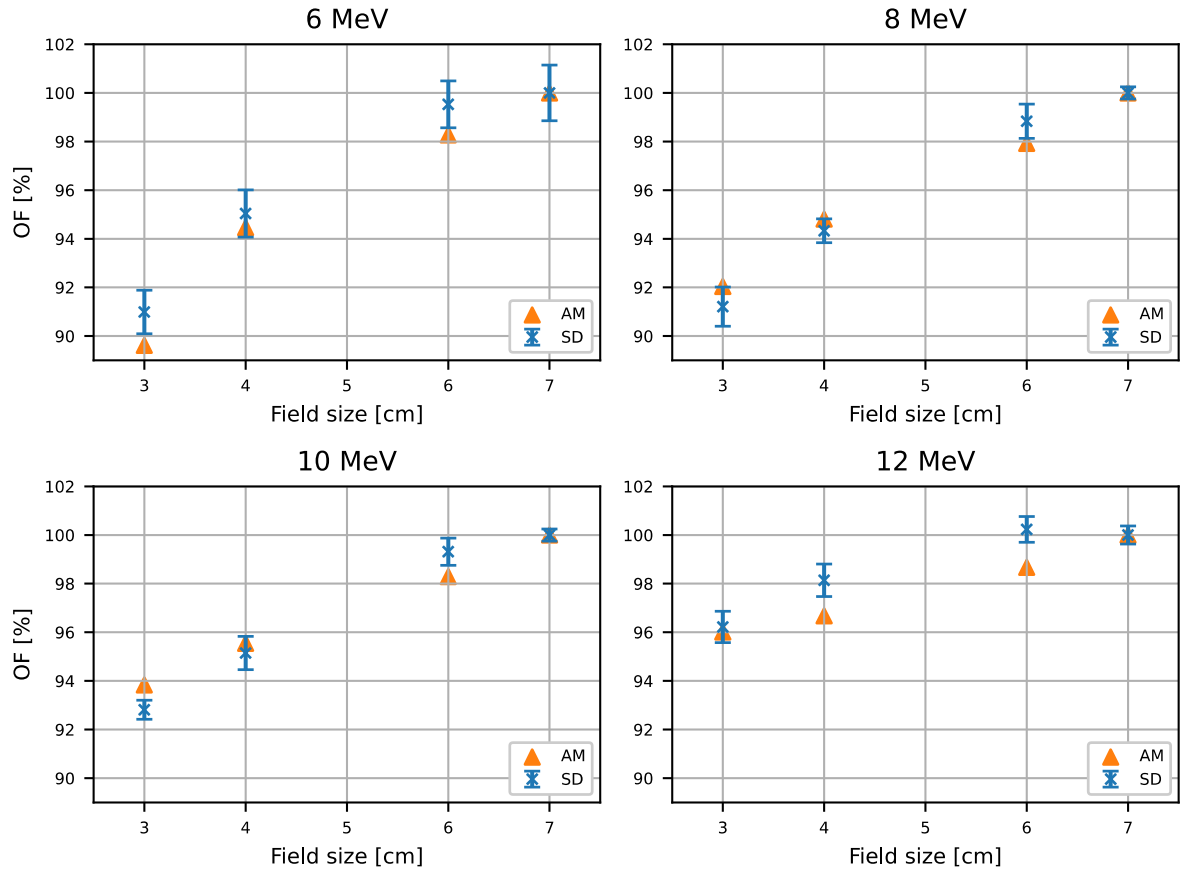


Fig. 5: Output-factor curve for 6 MeV to 12 MeV measured with AM, and SD. AM and SD align well and indicate comparable OF curves.

3.6 Surface dose measurements

Surface dose measurements are shown in Tab. 4. In the RW3 phantom, comparing against AM, all energies corresponded well between both detectors. There was no observable difference between the agreement at the surface or after the bolus material. Here, MAE was 0.9%. As expected, the dose increased with energy and depth. On the anthropomorphic (AP) phantom, agreement was observed, however the RF had a larger variance itself as compared to AM. Here, the relative MAE is 2.6%.

Tab. 4: Dose measurements for SD/reference on the surface and underneath 1cm bolus. For RW3, AM was used as reference and for the AP phantom (curved), RF was used as reference. All values in Gy.

Phantom/Depth	Incident electron beam energy			
	6 MeV	8 MeV	10 MeV	12 MeV
RW3/0 cm	1.42/1.42	1.56/1.54	1.63/1.60	1.75/1.72
RW3/1 cm	1.83/1.83	1.87/1.87	1.89/1.90	1.98/2.00
AP/0 cm	1.52/1.43	1.62/1.56	1.67/1.62	1.78/1.82
AP/1cm	1.84/1.82	1.87/1.91	1.88/1.92	1.97/1.99

4. Discussion

4.1 ACR and Dosimetric Characteristics

The determination of the ACR was crucial to correct for Cherenkov radiation and provide a detector signal that is proportional to dose. This is the case for all PSDs or scintillation detectors in general²¹. The observed value of 0.916 is, as expected, close to 1 and is comparable to the literature on PSDs^{25, 28, 29}. For a square 10×10 cm² field, the Cherenkov contribution contributed around 50% of the total signal. This means the Cherenkov contribution needed to be properly corrected for a reliable dose measurement. Since the vendor recommendations²³ advised Cherenkov contribution of less than 50% of the total signal, this translated to fields smaller than 10 cm length. Hence, no larger fields were considered in the present study.

For in vivo applications, this would be mostly avoidable by positioning the optical fiber at the shortest length of the field. Consequently, the relative importance can be minimized and potential errors avoided.

Regarding dosimetric properties of SD, four aspects were considered: Linearity, dose rate dependence, repeatability and isotropy. All of them were better than 1.5% and result in a total standard deviation of 1.8%.

The clinically acceptable dose-linearity of SD allowed for calibration using a constant calibration factor. In the regression, larger MU-values were important for the fit routine and a deviation for small MU-values was expected and observed in the experiments. The larger overall variation of the detector reading for small doses (<5 cGy) imposes the question whether these differences are due to the Linac or the detector. Preliminary tests performed on the same Linac indicated that an ionization chamber also showed larger relative standard deviation for such small doses. This suggests that the observed effect could at least partially be attributed to the Linac. This is in line with common recommendations regarding the commissioning and quality assurance³⁰. For most practical applications, doses below 5cGy are not considered relevant dose prescriptions for radiotherapy with static electron fields. Therefore, variations in the smaller MU-regime were not investigated further.

The performed experiments indicated less than 1.0% deviation of the detector reading based on the dose rate for clinically relevant doses. This does not necessarily mean that SD is fully dose rate independent. For the purposes of electron dosimetry in conventional clinical settings, this was deemed acceptable. Das et al., working with the same detector for photons, found a comparable dose rate dependence²⁴. Other PSDs were reported with dose rate dependences of 0.2 - 1.0%, meaning SD performed within this range^{25, 31, 32}. Since most publications considered photons irradiation, a strict comparison is difficult. When used at ultra-high dose rates, the behavior would have to be investigated further.

Small rotations can occur in particular during in vivo dosimetry and hence the angular dependence of SD was considered. The angular dependence was below 1% and allows for the use in clinical scenarios.

Overall, the detector characterization was in line with the findings for SD with photons^{24, 28, 29} and comparable to the performance of other PSDs^{25, 31, 32}.

4.2 Depth-Dose Curve and Profile Measurement

An investigation of PDDs and lateral profiles was used to determine two aspects: First, an accurate measurement of a PDD and profile by SD further indicates independence of dose-rate (as the effective

dose rate varies over the PDD and profile) and proper correction of the Cherenkov effect (since this can be expected to vary at throughout the measurement). Second, adequate determination of these beam-characteristics would enable the use of SD in quality assurance and commissioning procedures.

In this study, SD measured the PDD matching the reference from AM. Both visually in R_{80}/R_{50} , the discrepancies were below 0.5 mm. The only larger discrepancy was R_{max} for 12 MeV. This could be attributed to the plateau region around the maximum dose that is the largest for 12 MeV. Here, noisy SD data made a correct determination of the maximum dose and hence R_{max} difficult. Given that even for 12 MeV the other PDD characteristics aligned well, this was deemed acceptable.

Given the use-case of surface dosimetry, an important question to consider was the effect SD has on the PDD. Comparing PDD (as measured with AM) once in standard conditions and once with SD just above the water surface unveiled shifts of less than 1 mm but the functional behavior of the PDD remained the same.

The small shifts corresponded with the actual size of the plastic detector being 1 mm in diameter and scatter effects lowering the impact in depth. The fact that no further impact on the PDD was observed led to the conclusion that SD can be considered water-equivalent for dosimetric purposes. This means for a future in vivo application only the additional depth has to be taken into consideration without explicit modelling of the detector.

High fidelity measurement of PDDs were also found in other publications regarding SD other PSDs^{24,25}. The impact of the detector on the PDDs was to the best of our knowledge not considered in other publications, in particular for SD this was previously not shown. This was, however, essential to ensure in vivo measurements on the patient surface do not influence the dose delivery.

Profiles were acquired at depths of 0 cm and 1 cm to mimic the measurement situation at the surface and under 1 cm of bolus material – the realistic application scenario^{33,34}. Profile measurements were evaluated based on mean (absolute) differences. Mean absolute errors below 1.5% were acceptable for the profile measurements in particular as they were to be expected given the dosimetric characterization (see section 4.1). The mean error indicated that the difference between SD and ionization chamber profile measurements was noise-like and not systematic. No shifts or trends meant SD remained observable even in the penumbra region. It should be critically mentioned that the discrete measurement of profiles and PDD relied on the constant movement of the detector in the water phantom. While this was the case in the present study, this would be crucial to verify before use in quality assurance.

4.3 Small Field and Surface Dose Measurement

The determination of the OF curve in this study was used to ensure accurate dose measurement in small fields as they occur in typical in vivo settings^{35,36}. The choice to acquire the OF in 1 cm depth under clinical bolus material was motivated by the typical clinical treatment scenario. In an in vivo approach, SD could realistically be placed on top of the bolus or just underneath it on the patient skin but not in z_{ref} .

The use in small fields is essential for moving towards in vivo dosimetry as the treatment with square fields without further collimation is rare^{35,36}. In small fields, the alignment of the uncorrected SD measurement and AM was promising in this regard. While the consideration of the OF was less in depth as some more specialized publications³⁷, it was deemed sufficient for the use in vivo to estimate the correct dosimetric delivery.

Surface dose measurement showed excellent agreement of SD and the references both on the surface of the RW3 phantom and the anthropomorphic phantom. Here, the equivalence of the measurement set-ups was crucial, so for the curved geometry of the anthropomorphic phantom, RF was used as a

references even though they had a larger relative dosimetric error. To the best of our knowledge, the present study was the first time a PSD was shown to accurately measure surface doses. This is essential for the use for in vivo dosimetry.

Additionally, the fact that SD had negligible effect of the PDD was crucial for in vivo dosimetry as to not alter the dose to patient by measuring it.

Overall, SD demonstrated small deviations from ideal dosimetry less than 2%. As OF, PDDs and profiles are represented very well, we anticipate the use in vivo will be feasible.

5 Conclusion

The BluePhysics plastic scintillation detector provides accurate dosimetry for electron radiation in conventional clinical settings. Depth-dose curves, lateral profiles and output factors were in excellent agreement with standard reference detectors. Surface dose measurements in phantoms demonstrated excellent agreement with ionization chamber and film measurements. This allows for accurate in vivo dose measurements for a wide range of clinical scenarios with therapeutic electron beams.

Acknowledgments

The authors would like to thank Marcos Feijoo from BluePhysics for his technical support with the scintillation detector.

Data availability statements

The data acquired and analyzed in this study are available from the corresponding author upon reasonable request.

Author contribution statement

CB: Conceptualization, Data Curation, Formal Analysis, Investigation, Methodology, Visualization, Writing – Original Draft Preparation; FS: Conceptualization, Methodology, Supervision, Validation, Writing – Review & Editing; IG: Data Curation, Formal Analysis, Visualization, Writing – Review & Editing; HO: Methodology, Validation, Writing – Review & Editing; FG: Funding Acquisition, Supervision, Writing – Review & Editing; JF: Conceptualization, Methodology, Supervision, Validation, Writing – Review & Editing

Conflict of Interest Statement

FG reports research grants to his institution from Varian MS, Inc., Carl Zeiss Meditec AG, TME Pharma AG, OncoMAGNETx, Inc., Siemens Healthineers AG, and ELEKTA AB; consulting fees from CTK-Poliklinik GmbH, OncoMAGNETx, Inc., TME Pharma AG, and Cureteq AG; honoraria from Carl Zeiss Meditec AG, TME Pharma AG, OncoMAGNETx, Inc., AstraZeneca GmbH, and Siemens Healthineers AG; travel support from ELEKTA AB; patents with Carl Zeiss Meditec AG (US10857388B2) and University of Heidelberg (WO2023285170A1); expert roles with the Federal Joint Committee (G-BA, paid), yeswecan!cer (unpaid), and German Cancer Aid (unpaid); and stock ownership in TME Pharma AG.

Generative AI and Large Language Models

Generative AI technology (ChatGPT, OpenAI) was employed exclusively for editorial assistance, limited to spelling verification and refinement of readability. No generative AI tools were utilized in the conception, design, data acquisition, analysis, or interpretation of the study. The authors have thoroughly reviewed the manuscript and accept full responsibility for its content and integrity.

Bibliography

1. Hogstrom KR, Almond PR. Review of electron beam therapy physics. *Phys Med Biol.* 2006;51(13):R455-489. doi:10.1088/0031-9155/51/13/R25
2. Wolfe CM, Green WH, Hatfield HK, Shakar TJ, Baniahmad O, Cognetta AB. Multiple secondary cutaneous tumours following electron beam radiotherapy for cutaneous malignancies of the scalp. *Australas J Dermatol.* 2012;53(3):233-238. doi:10.1111/j.1440-0960.2012.00917.x
3. Wang D, Polignani JA. Quantitative approaches in electron skin collimation for the practical benefits. *J Appl Clin Med Phys.* 2024;25(4):e14236. doi:10.1002/acm2.14236
4. Gerbi BJ, Antolak JA, Deibel FC, et al. Recommendations for clinical electron beam dosimetry: supplement to the recommendations of Task Group 25. *Med Phys.* 2009;36(7):3239-3279. doi:10.1118/1.3125820
5. Sipilä P, Ojala J, Kajaluoto S, Jokelainen I, Kosunen A. Gafchromic EBT3 film dosimetry in electron beams - energy dependence and improved film read-out. *J Appl Clin Med Phys.* 2016;17(1):360-373. doi:10.1120/jacmp.v17i1.5970
6. 18. Bufacchi A, Carosi A, Adorante N, et al. In vivo EBT radiochromic film dosimetry of electron beam for Total Skin Electron Therapy (TSET). *Phys Med.* 2007;23(2):67-72. doi:10.1016/j.ejmp.2007.03.003
7. Nakajima E, Sato H. Characterization of a new radiochromic film (LD-V1) using mammographic beam qualities. *Z Med Phys.* 2025;35(2):169-176. doi:10.1016/j.zemedi.2023.05.004
8. Amin MN, Heaton R, Norrlinger B, Islam MK. Small field electron beam dosimetry using MOSFET detector. *J Appl Clin Med Phys.* 2010;12(1):3267. doi:10.1120/jacmp.v12i1.3267
9. Ciocca M, Piazzini V, Lazzari R, et al. Real-time in vivo dosimetry using micro-MOSFET detectors during intraoperative electron beam radiation therapy in early-stage breast cancer. *Radiother Oncol.* 2006;78(2):213-216. doi:10.1016/j.radonc.2005.11.011
10. Meiler RJ, Podgorsak MB. Characterization of the response of commercial diode detectors used for in vivo dosimetry. *Med Dosim.* 1997;22(1):31-37. doi:10.1016/s0958-3947(96)00152-5
11. Ade N, Du Plessis FCP. Electron beam dose perturbations caused by diode detectors used for in vivo dosimetry: Gafchromic film dose measurements in a realistic pelvic prosthesis phantom. *Radiation Physics and Chemistry.* 2018;151:232-238.
12. Pearce J, Thomas R, Dusauroy A. The characterization of the Advanced Markus ionization chamber for use in reference electron dosimetry in the UK. *Phys Med Biol.* 2006;51(3):473-483. doi:10.1088/0031-9155/51/3/001
13. Beddar AS, Mackie TR, Attix FH. Water-equivalent plastic scintillation detectors for high-energy beam dosimetry: I. Physical characteristics and theoretical consideration. *Phys Med Biol.* 1992;37(10):1883-1900. doi:10.1088/0031-9155/37/10/006
14. Beddar AS, Mackie TR, Attix FH. Water-equivalent plastic scintillation detectors for high-energy beam dosimetry: II. Properties and measurements. *Phys Med Biol.* 1992;37(10):1901-1913. doi:10.1088/0031-9155/37/10/007
15. Beaulieu L, Beddar S. Review of plastic and liquid scintillation dosimetry for photon, electron, and proton therapy. *Phys Med Biol.* 2016;61(20):R305-R343. doi:10.1088/0031-9155/61/20/R305
16. Dimitriadis A, Patallo IS, Billas I, Duane S, Nisbet A, Clark CH. Characterisation of a plastic scintillation detector to be used in a multicentre stereotactic radiosurgery dosimetry audit. *Radiat Phys Chem.* 2017;140:373-378.
17. Ciarrocchi E, Ravera E, Cavalieri A, et al. Plastic scintillator-based dosimeters for ultra-high dose rate (UHDR) electron radiotherapy. *Phys Med.* 2024;121:103360. doi:10.1016/j.ejmp.2024.103360
18. Vanreusel V, Gasparini A, Galante F, et al. Point scintillator dosimetry in ultra-high dose rate electron "FLASH" radiation therapy: A first characterization. *Phys Med.* 2022;103:127-137. doi:10.1016/j.ejmp.2022.10.005
19. Liu K, Holmes S, Schüler E, Beddar S. A comprehensive investigation of the performance of a commercial scintillator system for applications in electron FLASH radiotherapy. *Med Phys.* 2024;51(6):4504-4512. doi:10.1002/mp.17030
20. Baikalov A, Tho D, Liu K, Bartsch S, Beddar S, Schüler E. Characterization of a Time-Resolved, Real-Time Scintillation Dosimetry System for Ultra-High Dose-Rate Radiation Therapy Applications. *Int J Radiat Oncol Biol Phys.* 2025;121(5):1372-1383. doi:10.1016/j.ijrobp.2024.11.092

21. Clift MA, Sutton RA, Webb DV. Dealing with Cerenkov radiation generated in organic scintillator dosimeters by bremsstrahlung beams. *Phys Med Biol*. 2000;45(5):1165-1182. doi:10.1088/0031-9155/45/5/307
22. Beddar AS, Law S, Suchowerska N, Mackie TR. Plastic scintillation dosimetry: optimization of light collection efficiency. *Phys Med Biol*. 2003;48(9):1141-1152. doi:10.1088/0031-9155/48/9/305
23. Blue Physics LLC. Blue Physics model 11: instructions for use. Version 1.1. 2023
24. Das IJ, Sohn JJ, Lim SN, Sengupta B, Feijoo M, Yadav P. Characteristics of a plastic scintillation detector in photon beam dosimetry. *J Appl Clin Med Phys*. 2024;25(1):e14209. doi:10.1002/acm2.14209
25. Jacqmin DJ, Miller JR, Barraclough BA, Labby ZE. Commissioning an Exradin W2 plastic scintillation detector for clinical use in small radiation fields. *J Appl Clin Med Phys*. 2022;23(8):e13728. doi:10.1002/acm2.13728
26. Almond PR, Biggs PJ, Coursey BM, et al. AAPM's TG-51 protocol for clinical reference dosimetry of high-energy photon and electron beams. *Med Phys*. 1999;26(9):1847-1870. doi:10.1118/1.598691
27. Schneider F, Bauer CJ, Göbel ID, et al. Rapid and reversible adaptation of a clinical linear accelerator for electron FLASH radiotherapy. *Phys Med*. 2025;136:105032. doi:10.1016/j.ejmp.2025.105032
28. Oolbekkink S, van Asselen B, Woodings SJ, et al. Influence of magnetic field on a novel scintillation dosimeter in a 1.5 T MR-linac. *J Appl Clin Med Phys*. 2024;25(1):e14180. doi:10.1002/acm2.14180
29. Ferrer C, Huertas C, García D, Sáez M. Dosimetric characterization of a novel commercial plastic scintillation detector with an MR-Linac. *Med Phys*. 2023;50(4):2525-2539. doi:10.1002/mp.16204
30. Klein EE, Hanley J, Bayouth J, et al. Task Group 142 report: quality assurance of medical accelerators. *Med Phys*. 2009;36(9):4197-4212. doi:10.1118/1.3190392
31. Galavis PE, Hu L, Holmes S, Das IJ. Characterization of the plastic scintillation detector Exradin W2 for small field dosimetry. *Med Phys*. 2019;46(5):2468-2476. doi:10.1002/mp.13501
32. Carrasco P, Jornet N, Jordi O, et al. Characterization of the Exradin W1 scintillator for use in radiotherapy. *Med Phys*. 2015;42(1):297-304. doi:10.1118/1.4903757
33. Miéville FA, Pitteloud N, Achard V, et al. Post-mastectomy radiotherapy: Impact of bolus thickness and irradiation technique on skin dose. *Z Med Phys*. 2024;34(4):542-554. doi:10.1016/j.zemedi.2023.03.004
34. Kong D, Wu J, Kong X, et al. Effect of bolus materials on dose deposition in deep tissues during electron beam radiotherapy. *J Radiat Res*. 2024;65(2):215-222. doi:10.1093/jrr/rrae001
35. Arunkumar T, Supe SS, Ravikumar M, Sathiyam S, Ganesh M. Electron beam characteristics at extended source-to-surface distances for irregular cut-outs. *J Med Phys*. 2010;35(4):207-214. doi:10.4103/0971-6203.71763
36. Schulz JB, Gibson C, Dubrowski P, et al. Shaping success: clinical implementation of a 3D-printed electron cutout program in external beam radiation therapy. *Front Oncol*. 2023;13:1237037. doi:10.3389/fonc.2023.1237037
37. Gingras L, Cervantes Y, Beaulieu F, et al. Field output correction factors using a scintillation detector. *Med Phys*. 2025;52(6):4844-4861. doi:10.1002/mp.17729